Reorientation Effect Measurements on $Ba^{134, 136, 138}$ †

J. R. Kerns* and J. X. Saladin
University of Pittsburgh, Pittsburgh, Pennsylvania 15213
(Received 21 March 1972)

Using the O^{16} beam from the University of Pittsburgh tandem Van de Graaff accelerator, the angular distribution of the ratio of scattered ions exciting the first 2^+ state to elastically scattered ions has been measured. Values of the reduced transition probability $B(E2, 0^+ \rightarrow 2^+)$ and the static quadrupole moment Q_{2^+} of the first 2^+ state have been determined. The $B(E2, 0^+ \rightarrow 2^+)$ values obtained are 0.672 ± 0.016, 0.418 ± 0.011, and $0.221 \pm 0.009\ e^2 b^2$ for $Ba^{134, 136, 138}$, respectively. The spectroscopic quadrupole moments of the first 2^+ state of these nuclei are found to be -0.64 ± 0.14, -0.19 ± 0.17, and $-0.07 \pm 0.15\ e$ b, respectively. The results are compared with the predictions of various models.

1. INTRODUCTION

The present experiment was undertaken to complement an earlier experiment[1] which determined the static quadrupole moments of the first 2^+ states of $Nd^{144, 146, 148}$. It seemed interesting to compare the behavior of these nuclei with two, four, and six neutrons outside the $N = 82$ shell with that of the isotopes $Ba^{134, 136}$ which have four- and two-neutron holes and with Ba^{138}, where the $N = 82$ shell is closed.

In Sec. 3 the results of the present measurements together with the results of Simpson *et al.*[2] on Ba^{130} are compared with the predictions of various phenomenological models.

In addition the experiment aims at a determination of the sign of the interference contribution from the $2^{+\prime}$ (two-phonon) state and of the influence of the giant dipole resonance. This investigation is carried out for Ba^{134} and Ba^{136}.

2. EXPERIMENTAL PROCEDURE AND DATA EVALUATION

Enriched targets of $Ba(NO_3)_2$ were bombarded with oxygen beams of $+5e$, $+6e$, and $+7e$ charge obtained from the University of Pittsburgh three-stage tandem Van de Graaff accelerator. Typical beam currents varied between 0.5 and 1.2 μA on target.

The angular distribution of the ratio of the number of ions exciting the first 2^+ state to elastically scattered ions ($R_{exp} = d\sigma_{2^+}/d\sigma_{el}$) has been measured with an Enge split-pole spectrograph. The beam was defined by means of a $1\frac{1}{2}$-mm-wide × 2-mm-high slit which was followed by a slightly larger antiscattering slit. The O^{16} ions were detected by three position-sensitive detectors placed at the focal plane of the spectrograph. The use of three detectors allowed the simultaneous detection of the $+6e$, $+7e$, and $+8e$ charge states which comprise in most cases more than 96% of all scattered ions.

For more details of this part of the experimental setup we refer to some earlier work of our group.[3] The backward-angle data on Ba^{138} were obtained with ordinary solid-state detector spectroscopy. Four cooled (−30°C) Si surface-barrier detectors with depletion depths of 150 μ detected O^{16} ions at angles of 140, 150, 160, and −150°. The targets were produced by vacuum evaporation of isotopically enriched $Ba(NO_3)_2$ onto 10-μg/cm^2 carbon foils. Target thicknesses ranged from ~10 −15 μg/cm^2. Typical full width at half maximum resolutions were 120 keV for Ba^{134} and Ba^{136}, and 200 keV for Ba^{138}. The isotopic composition of the various targets is given in Table I.

In discussing the magnitude of various uncertainties we quote the numbers for Ba^{134}. The analysis of the other isotopes was carried out in an analogous fashion. First, the subtraction of contaminant contributions was performed using the supplier's analysis. Typical spectra are shown in Fig. 1. The uncertainty introduced by this subtraction, due to uncertainties in the isotopic abundances, was estimated to be $\pm 0.0023\ e^2 b^2$ and $0.023\ e$ b, for the $B(E2, 0^+ \rightarrow 2^+)$ and the quadrupole moment of the first 2^+ state. After subtraction of the impurities the ratio $d\sigma_{2^+}/d\sigma_{el}$ was determined from the areas under the inelastic and elastic peaks. Uncertainties in background subtraction under the inelastic peak constitute the dominant contribution to the over-all uncertainty in the experiment. The magnitude of this uncertainty which amounted to $\pm 0.012\ e^2 b^2$ for the $B(E2, 0^+ \rightarrow 2^+)$ and to $\pm 0.13\ e$ b for the quadrupole moment, was determined by extreme assumptions about the background under the inelastic peaks. We furthermore demanded that the shape of the inelastic peak after background subtraction was identical to that of the elastic peak. In evaluating the data the bombarding energy was taken to be the energy at the center of

TABLE I. Isotopic composition of targets in percent.

Target	Isotope 130	132	134	135	136	137	138
134	<0.05	<0.1	84.6 ± 0.2	4.1 ± 0.1	1.78 ± 0.1	1.63 ± 0.1	7.9 ± 0.2
136	<0.05	<0.05	<0.07	0.81 ± 0.05	92.9 ± 0.1	1.75 ± 0.05	4.54 ± 0.05
138	<0.01	<0.01	<0.01	<0.02	<0.02	0.20 ± 0.02	99.8 ± 0.02

the target. Uncertainties in target thickness, energy loss, and primary beam energy were estimated to give an over-all uncertainty in the effective bombarding energy of ±20 keV. The resulting uncertainties in the $B(E2, 0^+ \rightarrow 2^+)$ and Q_{2^+} are ±0.0023 e^2b^2 and ±0.020 eb, respectively.

The theoretical cross sections obtained from the coupled-channel calculations were appropriately averaged over the acceptance angle of the spectrograph. The scattering angle was known to ±0.1° leading to uncertainties of ±0.087 e^2b^2 and 0.0067 eb in the reduced transition probability and the quadrupole moment.

Since the charge-state distributions of O^{16} ions leaving a target are a function of energy, the charge-state distributions of the elastically scattered and inelastically scattered O^{16} ions differ slightly and the ratio $d\sigma_{2^+}/d\sigma_{el}$ for a single charge state is not the true ratio. By using the ratio of all inelastically to elastically scattered ions determined in the simultaneous accumulation of the $+6e$, $+7e$, and $+8e$ charge states, the maximum error introduced in R_{exp} by the exclusion of lower charge states is estimated at 0.3% for beam energies of 42 MeV and above.

Three O^{16} data points have been corrected for charge-state distributions, the 33-MeV data for Ba^{134} where approximately 7% of the scattered O^{16} ions were in the $+5e$ charge state and the Ba^{138} forward angle data where only the $+7e$ and $+8e$ charge states were accumulated. Information concerning charge-state distributions was taken from Northcliffe.[4] This correction resulted in a 0.6% increase in R_{exp} for the 33-MeV data. A summary of the experimentally determined ratios $R_{exp} = d\sigma_{2^+}/d\sigma_{el}$ is given in Table II.

In evaluating the experimental data the effects of atomic screening[3] and vacuum polarization[5] were taken into account. The former results in an increase of the effective bombarding energy of 78 keV, whereas the latter corresponds to a decrease of ~98 keV.

Since the computer code is based on the semiclassical approximation, quantum mechanical corrections using the tables of Pauli and Alder[6] were applied to the final results.

The experimental ratios R_{exp} were compared with the results of coupled-channel calculations in which the quadrupole matrix elements $M_{02} = \langle 0^+ \| \mathfrak{M}(E2) \| 2^+ \rangle$ and $M_{22} = \langle 2^+ \| \mathfrak{M}(E2) \| 2^+ \rangle$ were

TABLE II. Values of the experimental ratios $R_{exp} = d\sigma_{2^+}/d\sigma_{el}$.

Target	Projectile	Beam energy (MeV)	Lab scattering angle (deg)	R_{exp}
Ba^{134}	O^{16}	42.0	40.0	0.003 320 ± 0.000 040
	O^{16}	42.0	60.0	0.017 12 ± 0.000 25
	O^{16}	42.0	90.0	0.030 05 ± 0.000 44
	O^{16}	42.0	142.9	0.056 16 ± 0.000 65
	O^{16}	33.0	143.5	0.015 11 ± 0.000 28
	O^{16}	47.0	143.5	0.097 14 ± 0.000 87
Ba^{136}	O^{16}	42.0	60.6	0.005 149 ± 0.000 075
	O^{16}	42.0	100.6	0.015 76 ± 0.000 23
	O^{16}	42.0	140.5	0.022 96 ± 0.000 30
	O^{16}	47.0	144.4	0.044 45 ± 0.000 57
Ba^{138}	O^{16}	50.0	60.6	0.002 311 ± 0.000 053
	O^{16}	47.0	75.2	0.002 744 ± 0.000 078
	O^{16}	47.0	140.2	0.006 19 ± 0.000 15
	O^{16}	47.0	150.0	0.006 34 ± 0.000 12
	O^{16}	47.0	160.2	0.006 34 ± 0.000 15

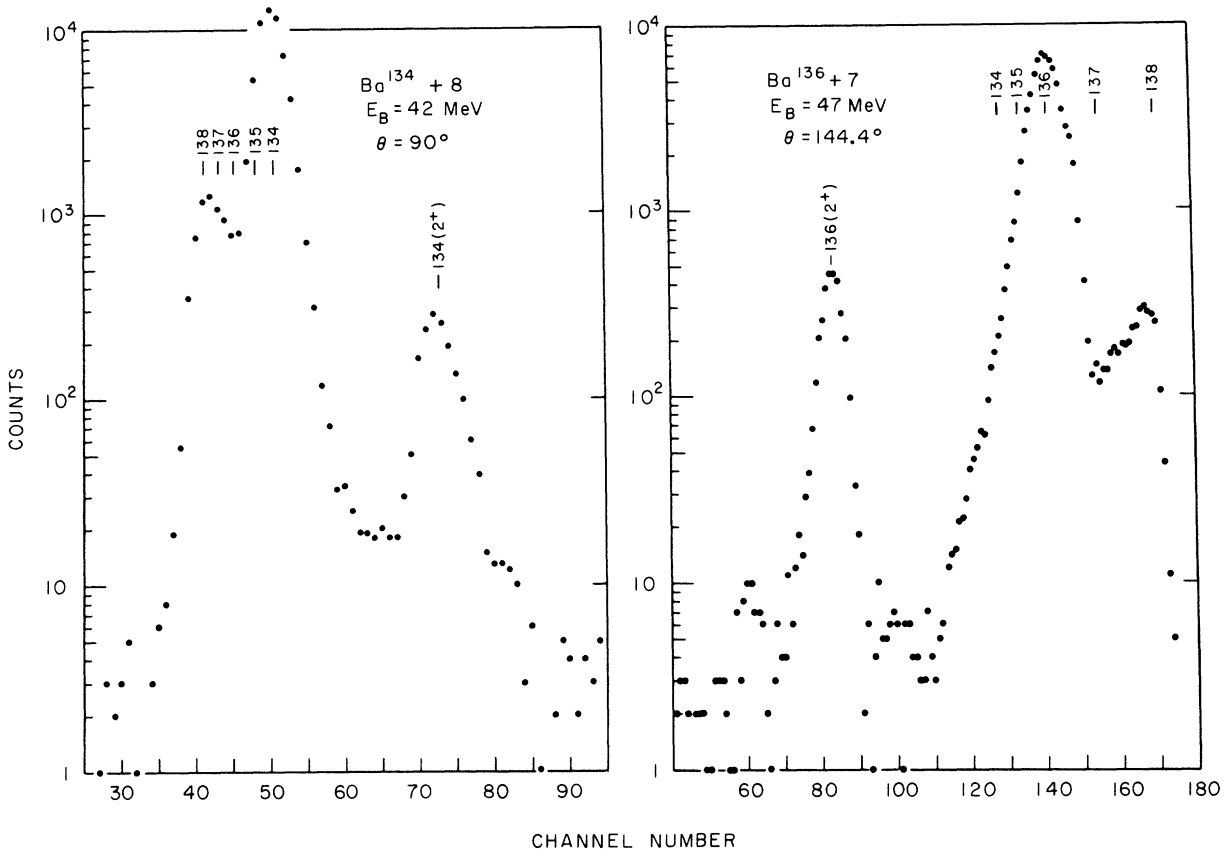

FIG. 1. Typical spectra obtained with the Enge split-pole spectrograph.

treated as variable parameters. It is well known that virtual excitation of the first 2^+ state via higher excited states can influence the analysis. The first few excited states of $Ba^{134, 136, 138}$ are shown in Fig. 2. Computer calculations showed, that low-lying 0^+ and 4^+ states introduce uncertainties of less than 0.015 eb in the evaluation of Q_{2^+}. Ba^{134} and Ba^{136} are known to have $2^{+\prime}$ states at 1.168 and 1.550 MeV, respectively. The branching ratios $B(E2, 2^{+\prime} \rightarrow 0^+)/B(E2, 2^{+\prime} \rightarrow 2^+)$ were available from γ-decay experiments[7,8] and are 0.005 ± 0.001 for Ba^{134} and 0.029 ± 0.006 for Ba^{136}. The branching ratio for Ba^{136} may be in error, since the mixing ratio $E2/M1$ has not been measured. In Ba^{134}, this transition is known to be essentially a pure $E2$ transition.[9]

To obtain explicit values for the reduced $E2$ transition probabilities, model predictions for the ratio $B(E2, 2^{+\prime} \rightarrow 2^+)/B(E2, 2^+ \rightarrow 0^+)$ have been used. The vibrational model predicts a value of 2 for this ratio. However, the asymmetric rotor model of Davydov and Chaban generally gives

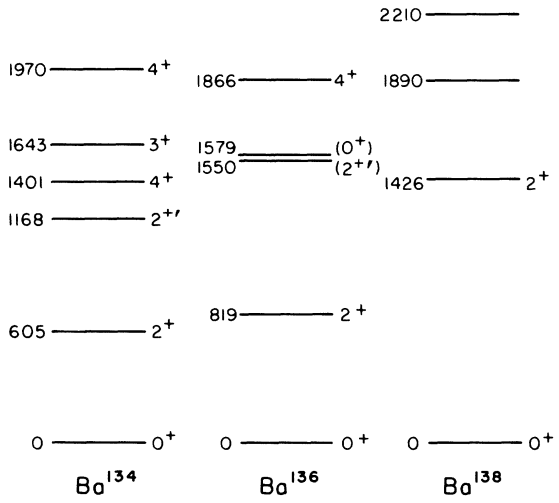

FIG. 2. Partial excitation spectra of Ba^{134}, Ba^{136}, and Ba^{138}.

TABLE III. Values of the $E2$ matrix elements $M_{02'}$ and $M_{2'2}$ in units of e b. See text.

	Ba^{134}		Ba^{136}	
Model	$M_{02'}$	$M_{2'2}$	$M_{02'}$	$M_{2'2}$
Harmonic vibrator	0.0897	±1.150	0.1560	±0.9170
Asymmetric rotor	0.0738	±0.9482	0.1200	±0.7230

better agreement with experiment. The two parameters of the model are the adiabaticity parameter μ and the asymmetry parameter γ which are fitted from the energy level spectrum. The values $\mu = 0.5$ and $\gamma = 26.5°$ characterize both nuclei and give

$$\frac{B(E2, 2^{+\prime} \to 2^{+})}{B(E2, 2^{+} \to 0^{+})} = 1.35 .$$

A summary of the matrix elements $M_{II'} = \langle I \| \mathfrak{M}(E2) \| I' \rangle$ adopted for the data evaluation is given in Table III.

3. RESULTS

The interference contribution due to the $2^{+\prime}$ states is proportional to the product $M_{02'} M_{2'2} M_{02}$. In general the sign of this triple product is not known, unless specific model assumptions are being made. Instead of using the sign of the triple product, it is convenient to conduct the discussion in terms of the four product $P_4 = M_{02'} M_{2'2} M_{02} M_{22}$ which is independent of a phase factor i^{λ} sometimes used in defining the matrix elements. Kumar[10] has shown, that under quite general assumptions, P_4 is negative, namely if the $2^{+\prime}$ state corresponds to a γ vibration or a two-phonon harmonic vibration with a small one-phonon admixture such as to make $M_{02'} \neq 0$. This result has been confirmed by our group for one case, namely Os^{188} by comparing the results of reorientation effect experiments with the results of Mössbauer studies.[11] We have nevertheless evaluated the data using either sign for P_4. The results are summarized in Table IV and some fits are shown in Fig. 3. In

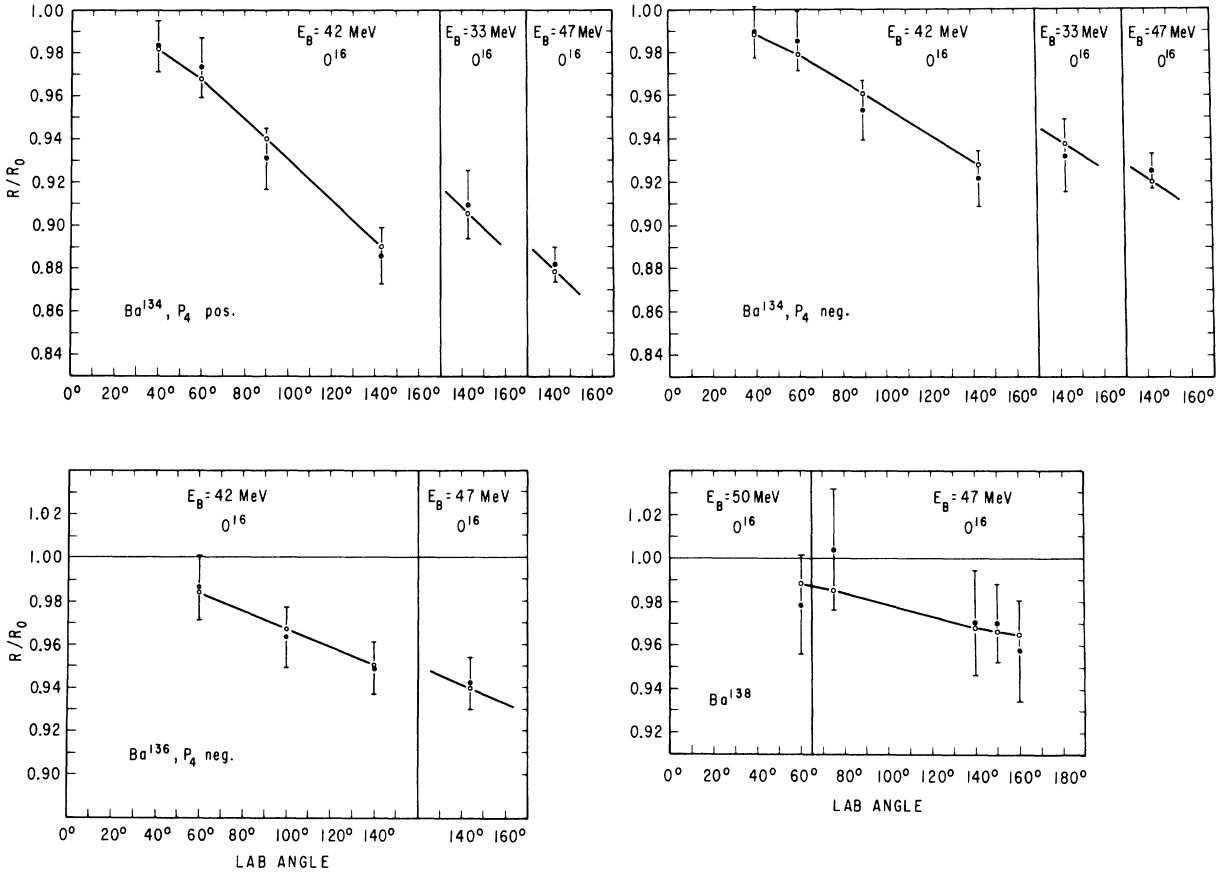

FIG. 3. Some least-square fits to R_{exp}/R_0, where $R_{exp} = (d\sigma_{2^+}/d\sigma_{0^+})_{exp}$ and $R_0 = d\sigma_{2^+}/d\sigma_{0^+}$ calculated, assuming $Q_{2^+} = 0$. The solid lines connect values R/R_0, where $R = d\sigma_{2^+}/d\sigma_{0^+}$ is calculated using the best value for Q_{2^+}.

TABLE IV: Results of least-squares analysis for either sign of P_4 and using various models (DC and HV) for estimating $M_{02'}$ and $M_{2'2}$. The column headed $Q_{2^+}^{QM}$ lists the quadrupole moments corrected for quantum mechanical effects.

Isotope	$B(E2, 0^+ \rightarrow 2^+)$ (e^2 b^2)	Q_{2^+} (e b)	$Q_{2^+}^{QM}$ (e b)	P_4	Model	χ^2	Degrees of freedom
Ba^{134}	0.672 ± 0.016	−0.71 ± 0.14	−0.68 ± 0.14	−	DC	0.764	4
	0.672 ± 0.017	−0.52 ± 0.16	−0.50 ± 0.16	+	DC	1.076	4
	0.671 ± 0.016	−0.73 ± 0.14	−0.70 ± 0.14	−	HV	0.818	4
	0.671 ± 0.017	−0.47 ± 0.16	−0.45 ± 0.16	+	HV	1.281	4
Ba^{136}	0.418 ± 0.011	−0.21 ± 0.17	−0.20 ± 0.17	−	DC	0.164	2
	0.417 ± 0.012	+0.02 ± 0.18	+0.02 ± 0.18	+	DC	0.496	2
	0.418 ± 0.011	−0.28 ± 0.17	−0.27 ± 0.17	−	HV	0.138	2
	0.417 ± 0.012	+0.11 ± 0.18	+0.11 ± 0.18	+	HV	0.674	2
Ba^{138}	0.221 ± 0.009	−0.11 ± 0.15	−0.11 ± 0.15				3

TABLE V. Results of least-squares analysis including η_0 as a variable parameter.

Isotope	$B(E2, 0^+ \rightarrow 2^+)$ (e^2 b^2)	$Q_{2^+}^{QM}$ (e b)	η_0	P_4	Model	χ^2	Degrees of freedom
Ba^{134}	0.689 ± 0.022	−0.51 ± 0.23	0.58 ± 0.53	−	DC	0.552	3
	0.673 ± 0.027	−0.48 ± 0.28	0.05 ± 0.70	+	DC	0.999	3
	0.689 ± 0.023	−0.52 ± 0.24	0.59 ± 0.56	−	HV	0.600	3
	0.668 ± 0.028	−0.49 ± 0.32	−0.10 ± 0.79	+	HV	1.272	3
Ba^{136}	0.434 ± 0.017	+0.02 ± 0.25	0.63 ± 0.51	−	DC	0.066	1
	0.431 ± 0.035	+0.24 ± 0.52	0.56 ± 1.30	+	DC	0.419	1
	0.434 ± 0.014	−0.04 ± 0.21	0.64 ± 0.37	−	HV	0.035	1
	0.443 ± 0.028	+0.47 ± 0.34	1.00 ± 1.30	+	HV	0.346	1

TABLE VI. "Best values" for $B(E2, 0^+ \rightarrow 2^+)$ and Q_{2^+}, and comparison with other measurements and the predictions of the Davydov-Chaban model. Columns 6 and 7 list the parameters of this model. Columns 8 and 9 represent the coefficients in a phonon mixing model. See text.

	$B(E2, 0^+ \rightarrow 2^+)$ Present work (e^2 b^2)	Previous values (e^2 b^2)	Q_{2^+} (e b)	Q_{2^+} Davydov-Chaban	γ	μ	a_1	a_2
Ba^{130}	...	1.36 [a]	−1.10 ± 0.34	−0.85	23.5°	0.4	0.858	0.51
Ba^{134}	0.672 ± 0.016	0.75 ± 0.23 [b]	−0.64 ± 0.14	−0.41	26.5°	0.5	0.916	0.40
Ba^{136}	0.418 ± 0.011	0.53 ± 0.16 [b]	−0.19 ± 0.17	−0.29	26.5°	0.5	0.99	0.14
Ba^{138}	0.22 ± 0.009 [b]	0.27 ± 0.08	−0.07 ± 0.15	...	...	...	0.998	0.06

[a] See Ref. 2.

[b] Values taken from D. G. Alkhazoz, B. S. Andreev, V. D . Vasilev, Y. P. Gangrskii, and I. Kh. Lemberg, Izv. Akad. Nauk SSSR, Ser. Fiz. 27, 1285 (1963) [transl.: Bull. Acad. Sci. USSR, Phys. Ser. 27, 1263 (1963)] .

order to illustrate the dependence on model assumptions in estimating the magnitude of the matrix element ($M_{2'2}$), the results are given in Table IV for the two models used, i.e., the Davydov-Chaban (DC) and the harmonic vibrator model (HV).

The χ^2 given in column 7 of Table IV clearly favor the solution with P_4 negative, even though the solution with P_4 positive cannot be entirely excluded.

On the basis of the theoretical arguments given above and in combination with these experimental results we feel, however, justified in favoring the solution for P_4 negative as the correct one. It is evident from Table IV that small differences in the choices for $M_{02'}$ and $M_{2'2}$ (DC) and (HV) have, compared with other uncertainties, little effect on the quadrupole moments and no effect on the $B(E2, 0^+ \to 2^+)$.

Calculations were performed in order to investigate the influence of virtual excitation via the giant dipole resonance. The deviation in the excitation probability P from first-order perturbation theory due to the giant dipole resonance was included, using the expression

$$\frac{\Delta P(E1)}{P(\text{first order})} = -1.98\times10^{-3}\,\frac{A_2 E(\text{MeV})}{Z_2(1+A_1/A_2)}\,\frac{\eta_0}{\gamma_{if}}\,\frac{f_{12}}{f_{11}} \tag{1}$$

derived by Eichler.[12,13] The mass numbers A_1 and A_2 refer to projectile and target, respectively, and η_0 is a nuclear structure parameter defined by

$$\left(\frac{5}{2}\right)^{1/2}\eta_0 \sum_n \frac{\langle 0\|\mathfrak{M}(E1)\|n\rangle\langle n\|\mathfrak{M}(E1)\|0^+\rangle}{E_n - E_0} \equiv \sum_n \frac{\langle 0^+\|\mathfrak{M}(E1)\|n\rangle\langle n\|\mathfrak{M}(E1)\|2^+\rangle}{E_n - E_0}.$$

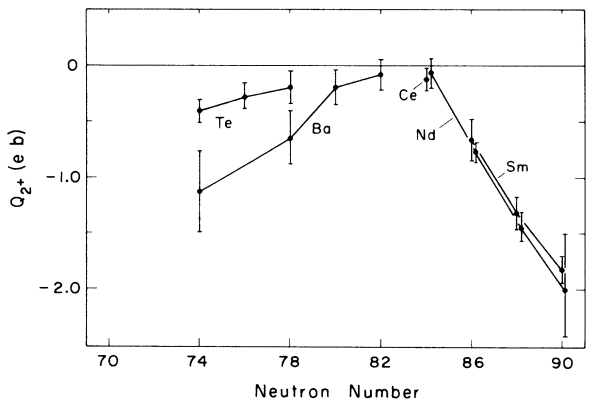

FIG. 4. Survey of Q_{2^+} in the $N=82$ region.

The quantity γ_{if} is defined by

$$B(E2, I_i \to I_f) = \gamma_{if}^2 \times 3\times10^{-5} A_2^{4/3}\, e\times10^{-48}\ \text{cm}^4$$

and the ratio f_{12}/f_{22} has been given by Eichler[12] as a function of the experimental conditions.

The parameter η_0 was treated as a variable to be determined from a least-squares fit. The results of this calculation are shown in Table V. Comparison with Table IV shows that the inclusion of η_0 as a variable parameter results in more positive quadrupole moments. The solutions with P_4 negative are again favored. Various theoretical estimates[14,15] yield $\eta_0 \sim 0.1$. The experiment seems to favor a somewhat larger value, is however within the rather large standard deviations consistent with the theoretical estimate.

In columns 2 and 4 of Table VI we summarize what we believe to be the best values for the quadrupole moments and the reduced transition probabilities. They are based on the solutions with P_4 negative, assuming $\eta_0 = 0.15$.

4. DISCUSSION

In Fig. 4 the quadrupole moments of the first 2^+ states of the Ba isotopes, including results on Ba^{130} by Simpson *et al.*,[2] are shown as a function of the neutron number, together with the results of earlier measurements of our group[1] and Gertzman *et al.*[16] on the Nd isotopes and results of various groups[17-19] on the isotopes of Ce, Te, and Sm. We note that the trend of the static quadrupole moment Q_{2^+} in the Ba isotopes is similar to that observed in the Nd and Sm isotopes. The magnitude of the static quadrupole moment of the Ba (Nd, Sm) isotopes increases rapidly as neutron pairs are removed from (added to) the $N=82$ closed neutron shell.

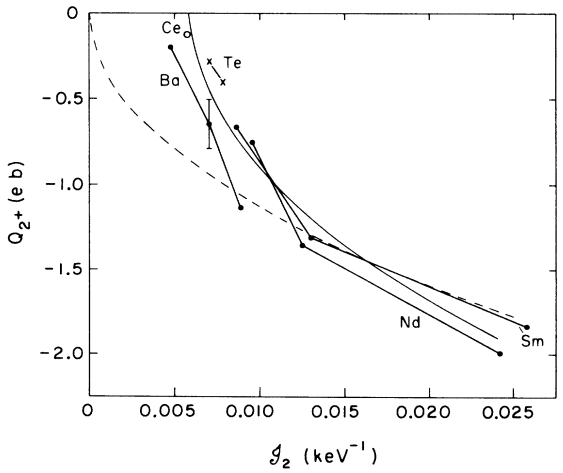

FIG. 5. Static quadrupole moments of the first 2^+ states versus moment of inertia ϑ_2.

It is interesting to correlate the data in this region with the variable-moment-of-inertia model of Mariscotti, Scharff-Goldhaber, and Buck.[20] In Fig. 5 we present a plot of the static quadrupole moment of the first 2^+ state versus the moment of enertia $\mathcal{I}_2$ of that state as calculated from the position of the 2^+, 4^+, and, where available, 6^+ state. There seems to be a striking correlation between the two quantities. Mariscotti, Scharff-Goldhaber, and Buck[20] suggested that there exists an empirical relationship between the moments of inertia and the intrinsic quadrupole moments describing the electromagnetic properties of the nucleus, i.e.,

$$Q_{0,02} = (39.4 \pm 2.6)\mathcal{I}_{02}^{1/2}, \tag{2}$$

$$\mathcal{I}_{02} = (\mathcal{I}_0 + \mathcal{I}_2)/2, \tag{3}$$

and

$$Q_{0,22} = k\mathcal{I}_2^{1/2}, \tag{4}$$

where $k = 39.4 \pm 2.6 \times 10^{-24}$ cm^2 keV$^{1/2}$. These intrinsic moments are related to the $B(E2; 0^+ \to 2^+)$ values and the spectroscopic quadrupole moment Q_{2^+} through

$$B(E2, 0^+ \to 2^+) = \frac{5}{16\pi} e^2 Q_{0,02}^2 \tag{5}$$

and

$$Q_{2^+} = -\tfrac{2}{7} Q_{0,22} = -11.25\,\mathcal{I}_2^{1/2}. \tag{6}$$

Relation (2) for transition moments has been verified to hold for a large set of data,[20] but the data on quadrupole moments were at that time rather scant. The dashed parabola in Fig. 5 represents relation (4) expressed in terms of static moments by means of Eq. (6). The relation works obviously exceedingly well for large values of $\mathcal{I}_2$ and Q_{2^+}, but the experimental quadrupole moments are considerably smaller than those predicted by Eq. (4) if the moments of inertia are smaller than about 0.007 keV^{-1}. However it should be pointed out that there is very little justification for Eq. (4). Equations (2) and (3) are purely empirical relationships and Eq. (4) represents an extrapolation of Eq. (2) for which there exists no theoretical foundation. The full parabola is an empirical fit to the data and is given by

$$Q_{2^+} = -a\sqrt{\mathcal{I}_2 - b}$$

with

$$a = 14.2 \pm 4.2 \text{ keV}^{-1/2}\ e\,\text{b}, \qquad b = 0.0059 \pm 0.0016 \text{ keV}^{-1}. \tag{7}$$

This relation suggests the possibility of a vanishing static quadrupole deformation in the presence of a finite moment of inertia.

A somewhat different approach is that of the axially not symmetric rotor model of Davydov and Chaban[21] which allows for rotation-vibration interactions. Column 5 of Table VI gives the prediction of this model whose parameters γ and μ which are listed in columns 6 and 7 were obtained from the position of the 2^+, $2^{+\prime}$, and 4^+ states in those nuclei. There seems to be fair agreement within the experimental uncertainties. Adjustments of γ by as little as 1° can in fact improve the agreement considerably, without altering the position of the excited states in an appreciable way.

Following a suggestion by Tamura and Udagawa[22] it is elucidating to consider the first two 2^+ states as orthogonal linear combinations of harmonic one- and two-phonon states $|1\rangle$ and $|2\rangle$, i.e.,

$$\psi(2^+) = a_1|1\rangle + a_2|2\rangle,$$

$$\psi(2^{+\prime}) = -a_2|1\rangle + a_1|2\rangle,$$

$$a_1^2 + a_2^2 = 1.$$

The magnitude of the static quadrupole moment of the first 2^+ state is given by

$$Q_{2^+} = \left(\frac{256\pi}{175}\right)^{1/2} a_1 a_2 [B(E2, 0^+ \to 2^+)]^{1/2}.$$

The required admixture a_2 of the two-phonon state in the wave function of the first 2^+ state is given in column 9 of Table VI. Using these coefficients a_2 one obtains predictions for the branching ratios $B(E2, 2^{+\prime} \to 2^+)/B(E2, 2^+ \to 0^+)$ and $B(E2, 2^{+\prime} \to 2^+)/B(E2, 2^{+\prime} \to 0^+)$ which are in qualitative agreement with typical values for nuclei in this region.

---

†Work supported by the National Science Foundation.

*Present address: Air Force Weapons Laboratory, Kirkland Air Force Base, New Mexico.

[1]P. A. Crowley, J. R. Kerns, and J. X. Saladin, Phys. Rev. C 3, 2049 (1971).

[2]J. J. Simpson, D. Eccleshall, A. J. Yates, and N. J. Freeman, Nucl. Phys. A94, 177 (1967).

[3]J. X. Saladin, J. E. Glenn, and R. J. Pryor, Phys. Rev. 186, 1241 (1969).

[4]L. C. Northcliffe, Ann. Rev. Nucl. Sci. 13, 67 (1963).

[5]L. L. Foldi and E. Erikson, Phys. Rev. 95, 1048 (1954).

[6]K. Alder and H. Pauli, Nucl. Phys. A128, 193 (1969).

[7]G. M. Julian and T. E. Fessler, Phys. Rev. 172, 1208 (1968).

[8]W. Gelletly, J. A. Moragues, M. A. Mariscotti, and W. R. Kane, Phys. Rev. (to be published).

[9]V. R. Potnis and Q. N. Rao, Nucl. Phys. 42, 620 (1963).

[10]K. Kumar, Phys. Letters 29B, 25 (1969).
[11]R. J. Pryor and J. X. Saladin, Phys. Rev. 1, 1573 (1970).
[12]J. Eichler, Phys. Rev. B133, 1162 (1964).
[13]We did not use the formulation given in the review article of J. deBoer and J. Eichler, in *Advances in Nuclear Physics*, edited by M. Baranger and E. Vogt (Plenum Press, 1968), Vol. 1, since it contains some misprints.
[14]deBoer and Eichler (Ref. 13).
[15]A. C. Douglas and N. McDonald, Phys. Letters 24B, 447 (1967).
[16]H. S. Gertzman, D. Cline, H. E. Gove, and P. M. S. Lesser, Nucl. Phys. A151, 282 (1971).
[17]G. Engler, Phys. Rev. C 1, 734 (1970).
[18]R. G. Stockstad and I. Hall, Nucl. Phys. A99, 506 (1967).
[19]D. Cline, P. Jennens, C. W. Towsley, and H. S. Gertzmann, Bull. Am. Phys. Soc. II, 16, 1156 (1971).
[20]M. A. J. Mariscotti, G. Scharff-Goldhaber, and B. Buck, Phys. Rev. 178, 1864 (1969).
[21]A. S. Davydov and A. A. Chaban, Nucl. Phys. 20, 499 (1960).
[22]T. Tamura and T. Udagawa, Phys. Rev. 150, 783 (1966).

PHYSICAL REVIEW C VOLUME 6, NUMBER 3 SEPTEMBER 1972

Prompt Gamma Rays Emitted in the Thermal-Neutron-Induced Fission of $^{235}U^{\dagger}$

Frances Pleasonton, Robert L. Ferguson, and H. W. Schmitt
Oak Ridge National Laboratory, Oak Ridge, Tennessee 37830
(Received 20 March 1972)

The average number and average energy of γ rays emitted within ~5 nsec after fission have been determined as functions of fragment mass and as functions of fragment mass and total kinetic energy in two-dimensional representations. In a four-parameter experiment, energies of coincident pairs of fission fragments were measured with surface-barrier detectors and γ-ray energies were measured with a large NaI(Tl) detector, which was located 89 cm from a thin ^{235}U target and positioned coaxially with the fragment detectors. The time difference between detection of a fission fragment and a γ ray was measured to allow time-of-flight discrimination against fission neutrons. The γ-ray data were analyzed with a "weighting method" proposed by Maier-Leibnitz to deduce average numbers and energies of γ rays from measured pulse heights. The Doppler shift in the laboratory angular distribution of γ emission was utilized to obtain the number and energy of γ rays as functions of single fragment mass. The results, for both average number and average energy as functions of single fragment mass, are characterized by a sawtooth behavior similar to that which is well known for neutron emission. The over-all average number and energy of γ rays emitted per fission were found to be 6.51 ± 0.3 and 6.43 ± 0.3 MeV, respectively, giving an average photon energy of 0.99 ± 0.07 MeV.

INTRODUCTION

The present work has been undertaken to study in detail the average number and average energy of γ rays emitted in the thermal-neutron-induced fission of ^{235}U, as functions of fragment mass and total kinetic energy. The experiment is a four-parameter experiment in which, for each event, the kinetic energies of both fragments, the amplitude of the γ-ray pulse, and the time between the fragment pulse and γ-ray pulse were recorded. The time measurement was incorporated so that contributions from delayed γ rays and neutrons could be minimized. Careful calibrations and determination of the γ-ray spectrometer's response matrix allowed absolute energies and numbers to be obtained.

In this paper we describe the experiment and data analysis in some detail and include a derivation and discussion of the method, certain aspects of which may have been unclear in an earlier report.[1] Results for ^{235}U thermal-neutron fission are given, together with a qualitative discussion of them. Experiments on other low-excitation fission cases are in progress; a future paper will present those results together with a more complete interpretation of all of the results.

γ-ray emission in fission is studied to obtain spectroscopic data for the fragments formed, to obtain information about the angular momentum with which the fragments are formed, and to determine the number and energy of γ rays for fission energy-balance considerations or for nuclear applications.

Generally, two different but complementary techniques are used. In the spectroscopic experiments, a high-resolution γ-ray detector (e.g., a lithium-drifted germanium detector) measures γ-ray ener-